

# Operando Investigations of Rare-Earth Oxycarbonate CO<sub>2</sub> Sensors <sup>†</sup>

Takuya Suzuki <sup>1,2,\*</sup>, Frieder Lauxmann <sup>3</sup>, Andre Sackmann <sup>1</sup>, Anna Staerz <sup>1</sup>, Udo Weimar <sup>1</sup>, Christoph Berthold <sup>3</sup> and Nicolae Barsan <sup>1</sup>

<sup>1</sup> Institute of Physical and Theoretical Chemistry, University of Tübingen, 72076 Tübingen, Germany; andre.sackmann@ipc.uni-tuebingen.de (A.S.); anna.staerz@ipc.uni-tuebingen.de (A.S.); upw@ipc.uni-tuebingen.de (U.W.); nb@ipc.uni-tuebingen.de (N.B.)

<sup>2</sup> Corporate R&D Headquarters, Fuji Electric Co. Ltd., Tokyo 1918502, Japan

<sup>3</sup> Applied Mineralogy, University of Tübingen, 72076 Tübingen, Germany; frieder.lauxmann@uni-tuebingen.de (F.L.); christoph.berthold@uni-tuebingen.de (C.B.)

\* Correspondence: takuya.suzuki@ipc.uni-tuebingen.de; Tel.: +49-(0)7071-29-78768

† Presented at the Eurosensors 2018 Conference, Graz, Austria, 9–12 September 2018.

Published: 26 November 2018

**Abstract:** In this work, we have succeeded in synthesizing monoclinic and hexagonal La<sub>2</sub>O<sub>2</sub>CO<sub>3</sub> using two different routes and revealed that both of them are sensitive to CO<sub>2</sub> to the same degree. Moreover, we observed that the resistance of the sensor based on hexagonal phase is much higher and more stable than the one of the sensors based on the monoclinic phase. Using Operando and time resolved XRD measurements, we have also demonstrated that the resistivity of the sensor based on monoclinic La<sub>2</sub>O<sub>2</sub>CO<sub>3</sub> increases because of the material transformation into the hexagonal phase during an exemplarily aging process.

**Keywords:** gas sensor; CO<sub>2</sub>; rare-earth oxycarbonate; operando investigation; XRD

---

## 1. Introduction

The CO<sub>2</sub> sensing is relevant not only in the conventional field of environmental safety, such as building and parking area management, but also in the agricultural and food businesses. The standard current technology is mainly NDIR, which is expensive, bulky, and hard to install. Obtaining low cost, simple and good performing chemoresistive CO<sub>2</sub> gas sensors has the potential to be a game changer.

Rare-earth oxycarbonates Ln<sub>2</sub>O<sub>2</sub>CO<sub>3</sub> (Ln = rare-earth element) have been proposed as promising chemoresistive materials for CO<sub>2</sub> sensors [1–5]. The already published results indicate monoclinic La<sub>2</sub>O<sub>2</sub>CO<sub>3</sub> as the most suitable material for CO<sub>2</sub> sensors among this family of materials. However, the monoclinic structure is metastable and could be transformed into the hexagonal structure. There are no reports about the sensing properties of the more thermally stable hexagonal La<sub>2</sub>O<sub>2</sub>CO<sub>3</sub>. Therefore, it is very important to find out more about the sensing properties and the stability of both structures.

In this paper, we have studied the issues of CO<sub>2</sub> sensing performance and thermal stability for both monoclinic and hexagonal La<sub>2</sub>O<sub>2</sub>CO<sub>3</sub>. To synthesize monoclinic and hexagonal La<sub>2</sub>O<sub>2</sub>CO<sub>3</sub> separately, two different preparation routes have been investigated. Such characterizations as DC resistance measurements, X-ray Diffraction (XRD) and Operando XRD have been conducted.

## 2. Materials and Methods

### 2.1. Material Synthesis and Sensor Fabrication

In many of the previous works [1–4], rare-earth oxycarbonates were formed from the hydroxides. However the hydroxides tend to become the oxides, which are thermally stable, during the heat treatments. In this study we have investigated the synthesis of La oxycarbonates through two different routes. One was from La hydroxide and the other was from La oxalate hydrate. Starting materials are powder or chunk, which are all commercially available. Each of them was put in an alumina boat and heated in the conditions as shown Table 1.

The powders after the heat treatment were mixed with propane-1,2-diol using a vibrating mill (30 Hz) for 30 min. The resulting pastes were screen printed onto alumina substrates provided with Pt interdigitated electrodes and Pt heaters. The gap of the interdigitated electrodes is 10  $\mu\text{m}$ . After the deposition of the sensing layer the substrates were dried in air at 70  $^{\circ}\text{C}$  for more than 12 h using an oven and then heated for 10 min using the same furnace and the conditions as its heat treatment.

**Table 1.** The conditions of heat treatments.

No.	Starting Material	Heat Treatment Conditions
1	La hydroxide	450 $^{\circ}\text{C}$ 18 h
2	La oxalate hydrate	450 $^{\circ}\text{C}$ 18 h
3	La oxalate hydrate	500 $^{\circ}\text{C}$ 18 h
4	La oxalate hydrate	500 $^{\circ}\text{C}$ 18 h

### 2.2. DC Resistance Measurements

A constant DC voltage was applied to the backside heater by a power supply, so as to maintain the sensor temperature at 250  $^{\circ}\text{C}$ , 300  $^{\circ}\text{C}$  or 350  $^{\circ}\text{C}$ . The heater voltage was calibrated in advance with a contactless thermometer. The DC resistance of sensor was measured every 10 s using an electrometer with varying humidity and  $\text{CO}_2$  concentration by a flow controller. The sensors were driven in humid air (50% relative humidity at 20  $^{\circ}\text{C}$ ) with 300 ppm  $\text{CO}_2$  for 12 h to stabilize the properties before the measurements of sensor responses.

### 2.3. XRD and Operando XRD

XRD was applied to characterize crystal structure of the powders after the heat treatment and sensors after the DC resistance measurements. The samples are scanned from 10 $^{\circ}$  to 60 $^{\circ}$  (2 $\theta$ ) by the X-ray with 1.5405980  $\text{\AA}$  wavelength (Cu- $\text{K}\alpha_1$  radiation).

XRD and DC resistance under operating conditions were measured simultaneously using Operando XRD apparatus. X-ray beam focused less than 1 mm in diameter was irradiated at the sensing layer through the X-ray optics and the transparency film of the sensor chamber. Then X-ray diffraction reached X-ray detector, which measured X-ray intensity from the angle (2 $\theta$ ) between 20 $^{\circ}$  and 60 $^{\circ}$  at once. The sensor electrodes and the heater electrodes were electrically connected to an electrometer and a power supply through the sensor holder, which was put in the sensor chamber connected to a gas flow controller.

## 3. Results and Discussion

### 3.1. DC Resistance Measurements

Figure 1a shows the sensor signals for the four types of sensors with varying operation temperature when they were operated under the atmosphere of 1000 ppm  $\text{CO}_2$  and 50% relative humidity at 20  $^{\circ}\text{C}$ . The sensor signal is defined as (1)

$$\text{Sensor signal} = R_g/R_0 \quad (1)$$

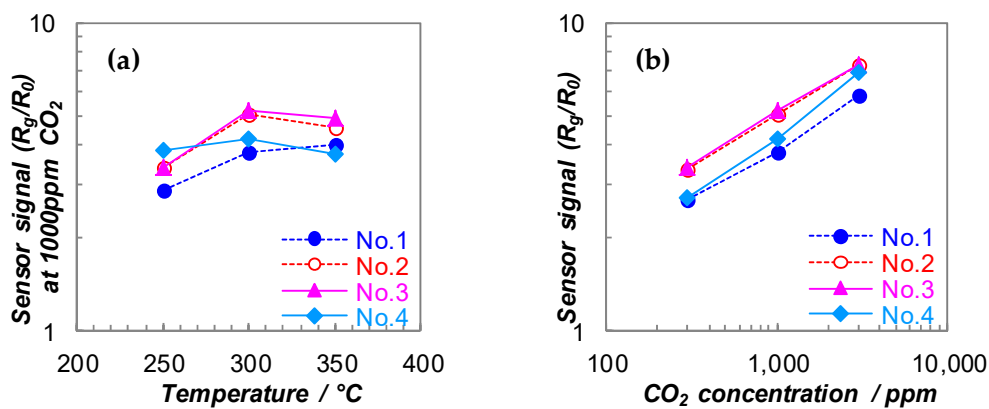
where  $R_g$  and  $R_0$  are the sensor DC resistance at a certain concentration of  $CO_2$  and at 0 ppm of  $CO_2$ , respectively. The sensor signal was the highest when they are operated at 300 °C for No. 2, No. 3 and No. 4. Only for No. 1, the sensor signal at 350 °C is a bit higher than that at 300 °C. Based on these results, 300 °C was chosen as the standard operation temperature for the further evaluation.

Figure 1b shows sensor signals of four types of sensors with varying  $CO_2$  concentration when they were operated at 300 °C. Every curve possessed a good linearity in a double logarithmic chart indicating that the sensor signal obeys power law as (2)

$$\text{Sensor signal} = A \times [\text{CO}_2 \text{ concentration}]^\alpha \tag{2}$$

where A and  $\alpha$  are constant values.

The sensor signals at a certain  $CO_2$  concentration were almost the same among four conditions. The sensitivity (corresponding to the gradient of sensor signal with  $CO_2$  concentration) of No. 4 is greater than those of the others.



**Figure 1.**  $CO_2$  Sensing properties: (a) Sensor signal at 1000 ppm  $CO_2$  vs operation temperature; (b) Sensor signal vs  $CO_2$  concentration.

In order to test the stability, a three day long aging process was performed in a high humidity and high  $CO_2$  concentration condition (80%rh@20 °C and 3000 ppm  $CO_2$ ) in air at an operation temperature of 350 °C.

Figure 2 shows the sensor resistances with varying  $CO_2$  concentration for the initial measurement and that after the aging process. With respect to the initial state, the sensor resistances of No. 1 and No. 4 were much higher than those of No. 2 and No. 3. After the aging process, the sensor resistances of No. 1 and No. 4 (initially hexagonal structure) remained unchanged while the sensor resistances of No. 2 and No. 3 (initially monoclinic structure) increased significantly.

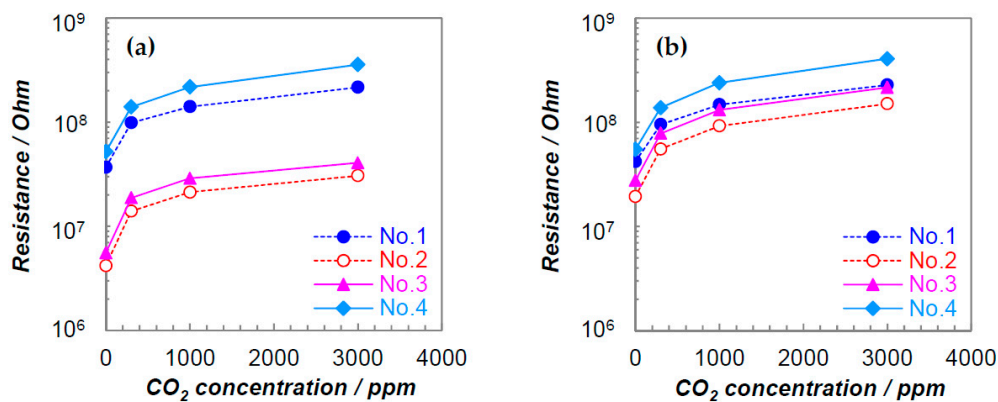


**Figure 2.** Sensor resistance vs  $CO_2$  concentration for (a) initial and (b) after aging.

### 3.2. XRD and Operando XRD

To investigate the differences in stability among the four types of sensors, XRD measurements were conducted before and after the aging process. The results are shown in Table 2 indicating that the hexagonal structures (No. 1 and No. 4) were preserved while the monoclinic structures (No. 2 and No. 3) were partly transformed into the hexagonal structure during the aging process.

To verify the correlation between the sensor resistance and the crystal structure, operando XRD measurements were performed using a sensor based on monoclinic  $\text{La}_2\text{O}_2\text{CO}_3$  (No. 3). The time dependent evolution of the sensor resistance and the XRD-patterns were measured simultaneously in humid air (80% relative humidity at 20 °C) in the presence of 3000 ppm  $\text{CO}_2$  at an operation temperature of 350 °C. Figure 3 shows the time variation of sensor resistance and XRD peak heights of hexagonal (103) and monoclinic (031) during the aging process, demonstrating that the resistance increased in direct correlation to the degree of the transformation from the monoclinic structure to the hexagonal structure.

**Table 2.** Results of XRD before and after the aging process. (h = hexagonal, m = monoclinic).

No.	Before	After
1	$\text{La}_2\text{O}_2\text{CO}_3$ (h)	$\text{La}_2\text{O}_2\text{CO}_3$ (h)
2	$\text{La}_2\text{O}_2\text{CO}_3$ (m)	$\text{La}_2\text{O}_2\text{CO}_3$ (m) $\text{La}_2\text{O}_2\text{CO}_3$ (h)
3	$\text{La}_2\text{O}_2\text{CO}_3$ (m)	$\text{La}_2\text{O}_2\text{CO}_3$ (m) $\text{La}_2\text{O}_2\text{CO}_3$ (h)
4	$\text{La}_2\text{O}_2\text{CO}_3$ (h)	$\text{La}_2\text{O}_2\text{CO}_3$ (h)

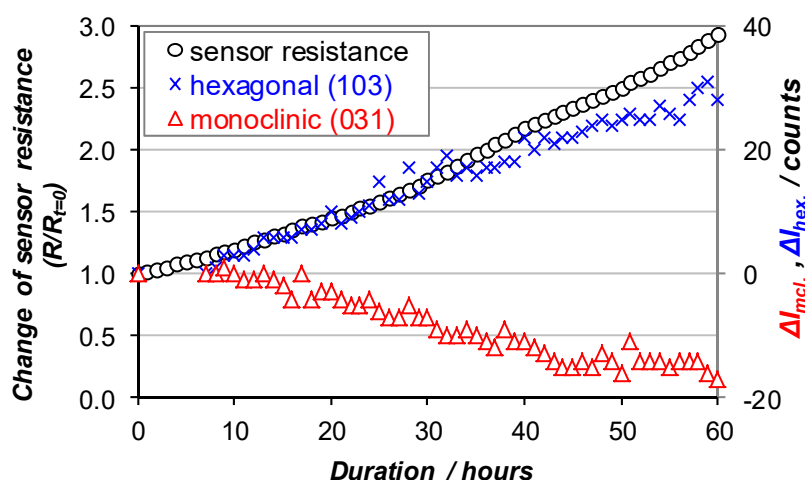


**Figure 3.** Time variations of sensor resistance and XRD peak height of  $\text{La}_2\text{O}_2\text{CO}_3$  hexagonal (103) & monoclinic (031) during the aging process.

### 4. Conclusions

We have succeeded for the first time in synthesizing monoclinic  $\text{La}_2\text{O}_2\text{CO}_3$  and hexagonal  $\text{La}_2\text{O}_2\text{CO}_3$  separately and showing clearly the sensing properties and stabilities of both structures.

La oxalate hydrate is a better precursor for synthesizing  $\text{La}_2\text{O}_2\text{CO}_3$  compared to La hydroxide which was used in many of previous works.

Hexagonal  $\text{La}_2\text{O}_2\text{CO}_3$  has better properties as a  $\text{CO}_2$  sensing material in terms of the sensitivity and the thermal stability than the monoclinic structure. The resistance of hexagonal  $\text{La}_2\text{O}_2\text{CO}_3$  is higher by approximately one digit, and the sensor signal is almost the same level compared to monoclinic  $\text{La}_2\text{O}_2\text{CO}_3$ . The Operando XRD method has revealed the direct correlation between the increase of sensor resistance and the degree of the transformation from the monoclinic structure to the hexagonal structure during the aging process.

**Conflicts of Interest:** The authors declare no conflict of interest.

## References

1. Djerdj, I.; Haensch, A.; Koziej, D.; Pokhrel, S.; Barsan, N.; Weimar, U.; Niederberger, M. Neodymium dioxide carbonate as a sensing layer for chemoresistive CO<sub>2</sub> sensing. *Chem. Mater.* **2009**, *21*, 5375–5381, doi:10.1021/cm9013392.
2. Haensch, A.; Koziej, D.; Niederberger, M.; Barsan, N.; Weimar, U. Rare earth oxycarbonates as a material class for chemoresistive CO<sub>2</sub> gas sensors. *Procedia Eng.* **2010**, *5*, 139–142, doi:10.1016/j.proeng.2010.09.067.
3. Chen, G.; Han, B.; Deng, S.; Wang, Y.; Wang, Y. Lanthanum dioxide carbonate La<sub>2</sub>O<sub>2</sub>CO<sub>3</sub> nanorods as a sensing material for chemoresistive CO<sub>2</sub> gas sensor. *Electrochim. Acta* **2014**, *127*, 355–361, doi:10.1016/j.electacta.2014.02.075.
4. Hirsch, O.; Kvashnina, K.O.; Luo, L.; Süess, M.J.; Glatzel, P.; Koziej, D. High-energy resolution X-ray absorption and emission spectroscopy reveals insight into unique selectivity of La-based nanoparticles for CO<sub>2</sub>. *Proc. Natl. Acad. Sci. USA* **2015**, *112*, 15803–15808, doi:10.1073/pnas.1516192113.
5. Kodu, M.; Avarmaa, T.; Mändar, H.; Saar, R.; Jaaniso, R. Structure-Dependent CO<sub>2</sub> Gas Sensitivity of La<sub>2</sub>O<sub>2</sub>CO<sub>3</sub> Thin Films. *J. Sens.* **2017**, doi:10.1155/2017/9591081.



© 2018 by the authors. Licensee MDPI, Basel, Switzerland. This article is an open access article distributed under the terms and conditions of the Creative Commons Attribution (CC BY) license (<http://creativecommons.org/licenses/by/4.0/>).